SUPPORTING INFORMATION FOR:

Physically crosslinked polyacrylates by quadruple hydrogen bonding side chains

Jente Verjans,[1] Alexis André,[2,3] Tomáš Sedlačík,[1] Resat Aksakal,[4] Evelyne Van Ruymbeke,[2,*] and Richard Hoogenboom[1,*]

[1] Supramolecular Chemistry Group, Centre of Macromolecular Chemistry (CMaC), Department of Organic and Macromolecular Chemistry, Ghent University, B-9000 Ghent, Belgium.

[2] Bio- and Soft Matter, Institute of Condensed Matter and Nanosciences, Université catholique de Louvain, B-1348 Louvain-la-Neuve, Belgium.

[3] Department of Chemical Engineering, Katholieke Universiteit Leuven, B-3001 Leuven, Belgium.

[4] Polymer Chemistry Research Group, Centre of Macromolecular Chemistry (CMaC), Department of Organic and Macromolecular Chemistry, Ghent University, B-9000 Ghent, Belgium.

Table of Contents

1 Experimental Methods

1.1 Materials

Unless stated otherwise, all reagents were obtained from commercial sources and used without further purification. All high-performance liquid chromatography (HPLC) grade solvents were purchased from Sigma-Aldrich: acetonitrile (ACN), chloroform ($CHCl_3$), diethyl ether (Et_2O), methanol (MeOH), dichloromethane (DCM), *N,N*-dimethylacetamide (DMA), ethyl acetate (EtOAc), triethylamine (Et_3N), and tetrahydrofuran (THF), Biosolve: *N,N*-dimethylformamide (DMF) or Fisher Scientific: toluene.

Dry solvents: ACN, Et_3N, and THF were obtained from a custom-made JW Meyer solvent purification system and dried over aluminum oxide columns. Argon (Ar) (Alphagaz 1) was purchased from Air Liquide and used as supplied. Magnesium sulfate ($MgSO_4$), sodium chloride (NaCl), sodium bicarbonate ($NaHCO_3$), hydrochloric acid (HCl) (37% in water), guanidine carbonate (99%) and ammonium hydroxide (NH_4OH) (35% in water) were purchased from Fisher Scientific.

Allyl alcohol (98.5%), ethyl *α*-bromoisobutyrate (EBiB) (98%), copper(II) bromide ($CuBr_2$) (99%), tris[2-(dimethylamino)ethyl]amine (Me_6-Tren) (97%), methyl acrylate (MA) (99%), *n*-butyl acrylate (BA) (99%), 1-butanethiol (99%), ethanethiol (97%) and triazabicyclodecene (TBD) (98%) were purchased from Sigma-Aldrich. Inhibitor removal of MA and BA prior to polymerization was done by flowing the monomer over a plug of basic alumina. 1,1'-carbonyldiimidazole (CDI) (97%) and cysteamine hydrochloride (95%) were purchased from TCI Chemicals. Trifluoroacetic acid (TFA) (99.5%) was purchased from Biosolve. Bio-Beads S-X1 was purchased from Bio-Rad. 6-(2-Ethylpentyl)isocytosine and 6-(2-ethylpentyl)imidazolide were synthesized according to literature procedures.[1]

1.2 Equipment

^{1}H nuclear magnetic resonance (^{1}H NMR) spectra were recorded on a Bruker Avance 300 Ultrashield or Bruker Advance II 400 MHz spectrometer at room temperature. The compounds were dissolved in either chloroform-*d* ($CDCl_3$) or dimethylsulfoxide-d_6 (DMSO-d_6) from Euriso-top. The chemical shifts (δ) are given in parts per million (ppm) and referenced against tetramethylsilane, with the residual $CHCl_3$ and DMSO signals at 7.26 ppm or 2.50 ppm, respectively. The PMA and PBA homopolymers were characterized on a Size Exclusion Chromatography (SEC) system from Waters equipped with a Waters 1515 isocratic pump, Waters 2410 refractive index detector (24 °C), Waters 717plus autosampler and a Waters 2487 dual λ absorbance UV detector and column oven. For separation, a three-column setup was used with one SDV 3 µm, 8×50 mm precolumn and two SDV 3 µm, 1000 Å, 8×300 mm columns supplied by PSS, Germany. Tetrahydrofuran (THF) stabilized with butylated hydroxytoluene (BHT, HPLC-SEC grade) supplied by Biosolve was used at a flow rate 1.0 mL/min. Calibration was carried out by three injections of a mixture of narrow polystyrene standards ranging from 162 to 38640 g/mol. Polymer samples were diluted in THF to a 2 mg/mL concentration and filtered over a short plug of basic aluminium oxide to remove trace amounts of catalyst before submitted for analysis.

The PMA-UPy and PBA-UPy polymer networks were characterized on an Agilent 1260-series HPLC system equipped with a 1260 online degasser, a 1260 ISO-pump, a 1260 automatic liquid sampler (ALS), a thermostated column compartment (TCC) at 50°C equipped with two PLgel 5 µm mixed-D columns and a precolumn in series, a 1260 diode array detector (DAD) and a 1260 refractive index detector (RID). The used eluent was DMA containing 50 mM of LiCl at

a flow rate of 0.500 mL/min. The spectra were analysed using the Agilent Chemstation software with the GPC add-on. Number average and weight average molar mass values (M_n and M_w, respectively) and dispersity (Đ) values were calculated against PMMA standards from PSS.

Centrifugation was performed on an ALC multispeed refrigerated centrifuge PK 121R from Thermo Scientific using 50 mL centrifuging tubes with screw caps from VWR or 15 mL high-clarity polypropylene conical tubes from Falcon. Thermogravimetric analysis (TGA) was performed with a Mettler Toledo TGA/SDTA851e instrument under nitrogen atmosphere at a heating rate of 10 °C/min from 25 to 800 °C.

Differential scanning calorimetry (DSC) analyses were performed with a Mettler Toledo instrument 1/700 under nitrogen atmosphere at a heating rate of 10 °C/min.

Dynamic mechanical thermoanalysis (DMTA) was performed on a Mettler-Toledo DMA/SDTA861e using shear mode on 8 mm disks. The temperature was increased from -50 °C to 150 °C at a heating rate of 3 °C/min.

Rheological experiments were measured on an Anton Paar MCR 302 rheometer equipped with a CTD 450 oven using a parallel plate geometry and 8 mm disk samples. Unless specified otherwise, the experiments were performed using a normal force of 0.02 N, an angular frequency of 10 rad/s, and a strain of 0.1%.

Amplitude sweeps were performed from 0.1 to 100% with a constant angular frequency of 10 rad/s. Frequency sweeps were carried out with an angular frequency ranging from 600 to 0.001 rad/s at constant temperature and the measurement was stopped when a cross-over of storage and loss modulus (G' and G'', respectively) appeared.

Uniaxial tensile testing was performed on a Tinius-Olsen H10KT tensile tester equipped with a 100 N load cell using ASTM standard type IV dog bones (ISO 527-2-2B). The dog bone-shaped samples had an effective gauge length of 12 mm, a width of 2 mm, and a thickness of ±2 mm, and they were cut using a Ray-Ran hand operated cutting press. The tensile measurements were performed using a preload of 0.05 N and a pulling speed of 10 mm/min until sample failure. The stress (σ) was recorded as a function of strain (ε). The Young's modulus (E) was determined from the initial linear part of the stress−strain curves using the machine software, typically in a strain range of 0.5-2%. Reported values: elongation (%), stress at break (MPa), and Young's modulus (MPa) are the result of single measurement due to limited amount of material available.

Samples for DMTA, rheology and tensile testing were compression molded with a heat press at a temperature of 80-100 °C and a pressure of 1-2 metric tons for 5 minutes.

1.3 Methods

1.3.1 Synthesis of 2-mercaptoethylureido-6-(2-ethylpentyl)pyrimidone (UPy-SH)

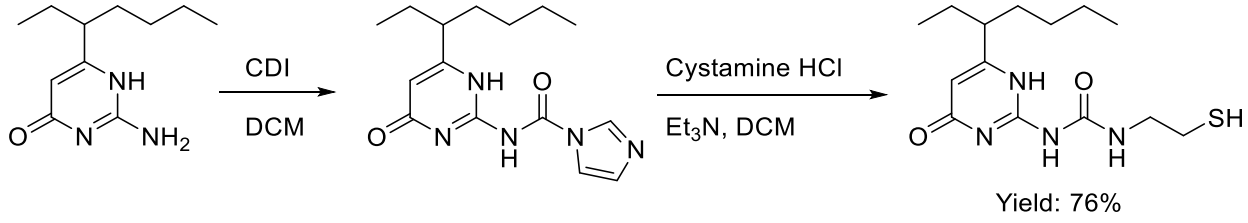

Yield: 76%

The UPy units were prepared as reported by Keizer et al.[1] (2-Ethylpentyl)isocytosine (10.13 g, 48.4 mmol, 1 eq) and CDI (10.43 g, 64.4 mmol, 1.33 eq) were dissolved in dry DCM (51 mL) and the resulting yellow solution was stirred overnight at room temperature under inert atmosphere. The reaction mixture was then diluted with DCM (175 mL) and washed with water (50 mL), brine (50 mL) and dried over $MgSO_4$. The solvent was removed under reduced pressure and the product was used in the next step without further purification.

6-(2-ethylpentyl)imidazolide (14.68 g, 48.4 mmol) was dissolved in dry dichloromethane (70 mL), cysteamine hydrochloride(6.74, 59.3 mmol, 1.2 eq), and triethyl amine (8.5 mL, 1.2 eq) were added and the resulting dark orange solution was stirred at room temperature overnight. The reaction mixture was then diluted with dichloromethane (70 mL) and washed with 1M HCl solution (50 mL), saturated $NaHCO_3$ solution (50 mL), and brine (50 mL), dried with $MgSO_4$ and evaporated under reduced pressure. The product was further purified *via* column chromatography (silica, gradient 1 to 2 % methanol in chloroform), resulting in a light-yellow oil, which crystallized to a white solid over time (yield: 11.73 g, 76%).

^{1}H NMR (300 MHz, $CDCl_3$): δ 13.12 (s, 1H), 11.99 (s, 1H), 10.49 (s, 1H), 5.82 (s, 1H), 3.47 (td, *J* = 7.5, 7.0, 5.5 Hz, 2H), 2.74 (dt, *J* = 8.1, 7.0 Hz, 2H), 2.31 (ddd, *J* = 9.0, 5.6, 3.5 Hz, 1H), 1.83 – 1.43 (m, 5H), 1.40 – 1.14 (m, 4H), 0.88 (m, 6H).

1.3.2 General conditions for the polymerization of Methyl acrylate

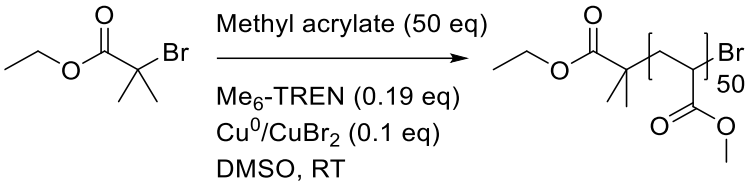

For a typical polymerization, $CuBr_2$ (0.1 eq), DMSO (1:1, $V_{monomer}$:$V_{solvent}$), Me_6TREN (0.19 eq), MA (20 g, 50 eq), and initiator (EBiB) (1.0 eq.) were added to a Schlenk tube containing a stirrer bar. The Schlenk tube was subsequently sealed with a rubber septum, lowered into an oil bath set to 25 °C and degassed with argon for 30 minutes. At the same time, a 5 cm piece of copper wire was preactivated in 10 mL HCl (conc. 37%) for 20 minutes, then washed with deionized water and acetone and dried under argon. The activated copper wire was then immediately transferred to the Schlenk tube containing the polymerization mixture to start the reaction. The reaction mixture was allowed to polymerize for 16 h (ρ = 99%, $M_{n,SEC}$ = 4700 g/mol, Đ = 1.06)

1.3.3 General conditions for the photopolymerization of Butyl acrylate

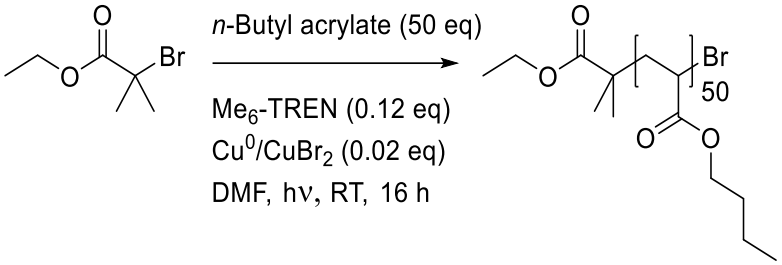

For a typical polymerization, $CuBr_2$ (0.02 eq.), DMF (1:1, $V_{monomer}$:$V_{solvent}$), Me_6TREN (0.12 eq.), BA (20 g, 50 eq.) and initiator (EBiB) (1.0 eq.) were added to a vial containing a stirrer bar. The vial was subsequently sealed with a rubber septum and degassed with argon for 30 minutes. The reaction mixture was allowed to polymerize for 16 h under exposure to UV light. (ρ = 94%, $M_{n,SEC}$ = 6600 g/mol, Đ = 1.05)

1.3.4 General conditions for the purification of bromine terminated polymers

Upon completion of polymerization, respective polymers were precipitated in an excess amount of cold methanol/water solution. The resulting suspension was carefully decanted, the polymer redissolved in THF and the precipitation repeated. The resulting suspension was once again decanted and the polymers dried in a vacuum oven to constant weight.

1.3.5 General conditions for the polymer end group modification

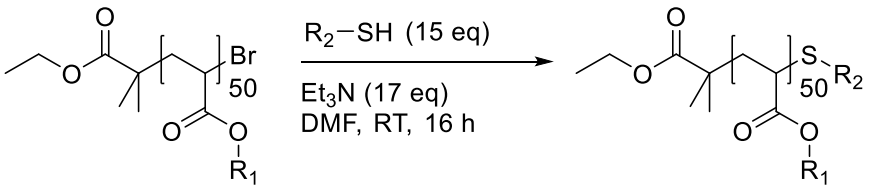

PMA_{50} or PBA_{50} (1 eq), 1-butanethiol or ethanethiol (15 eq), respectively, triethyl amine (17 eq), and dry DMF (1:5 *v*/*v*) were all added in a sealed vial under Argon and the reaction was left to proceed overnight for approximately 16 h. The reaction mixture was then concentrated under vacuum at 50 °C, dissolved in ethyl acetate and worked up by extraction

using 3 x 1 M NaOH and 3 x 1 M HCl. The organic layer was then dried over $MgSO_4$, filtered and the solvent was removed under vacuum. The polymers were dried in a vacuum oven to constant weight before being used for further modification. Specification of used polymers: PMA_{50}: $M_{n,SEC}$ = 4800 g/mol, Đ = 1.06 and PBA_{50}: $M_{n,SEC}$ = 6800 g/mol, Đ = 1.05.

1.3.6 General conditions for the stoichiometrically controlled transesterification of PMA

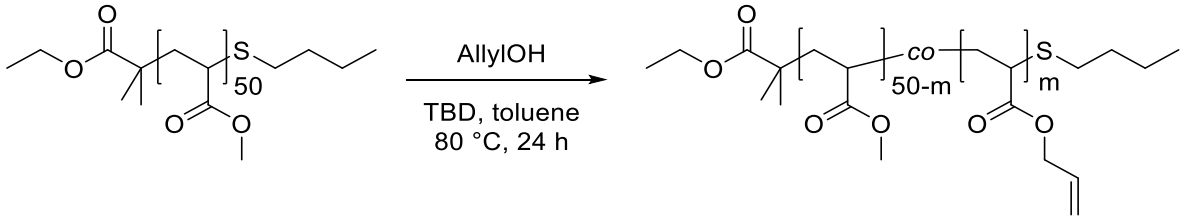

The PMA was functionalized with allyl alcohol via TBD-catalyzed transesterification, as reported by Van Guyse et al.[2] PMA (1 eq methyl esters) and allyl alcohol (0.062, 0.156 or 0.260 eq) were dissolved in toluene (0.5 M methyl esters). The solution was degassed by argon bubbling for 30 minutes, TBD (5 mol%) was added and the resulting solution was heated to 80 °C overnight. Once completed, Dowex 50W X8 resin (50 mg/g of PMA) was added and the mixture was stirred for 24 h to remove residual catalyst. The resin was filtered and the solvent was removed under reduced pressure, yielding the purified functionalized polymer.

Calculation of conversion: The conversion/fraction was calculated by using the signals of the CH_2-O groups of the formed allyl ester at 4.5 ppm. This signal, which integrates for 2 protons and the signal of the methyl ester present at 3.6 ppm, which integrates for 3 protons were utilized in the following calculation:

$$Conversion = \frac{\frac{Integral\ CH_2}{2}}{\frac{Integral\ CH_2}{2} + \frac{Integral\ CH_3}{3}}$$

1.3.7 General conditions for the stoichiometrically controlled transesterification of PBA

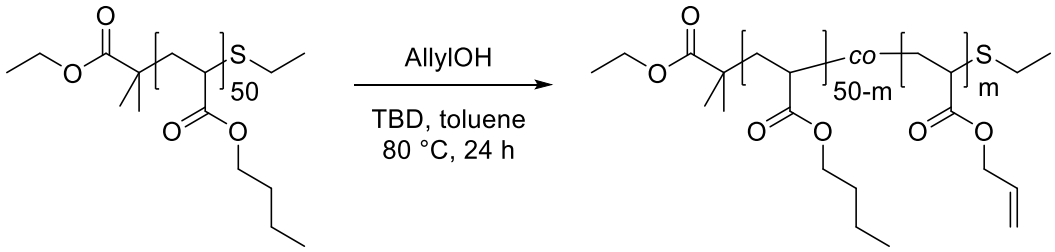

The PBA was functionalized with allyl alcohol via TBD-catalyzed transesterification, as reported by Van Guyse et al.[2] PBA (1 eq butyl esters) and allyl alcohol (0.062, 0.156 or 0.260 eq) were dissolved in toluene (0.5 M methyl esters). The solution was degassed by argon bubbling for 30 minutes, TBD (5 mol%) was added and the resulting reaction mixture was heated to 80 °C overnight. After 24 hours, Dowex 50W X8 resin (50 mg/g of PBA) was added and the mixture was stirred for another 24 h to remove residual catalyst. The reaction mixture was allowed to cool down to room temperature and filtered to remove the resin. Finally, solvent removal under reduced pressure yielded the purified polymer.

The same fitting curve was used to determine the stoichiometric ratios for transesterification of PBA, so the table mentioned above for PMA is identical for PBA.

Calculation of conversion: identical to PMA-Allyl as mentioned above.

1.3.8 General conditions for the thiol-ene coupling of UPy-SH onto the allyl esters of the polymers

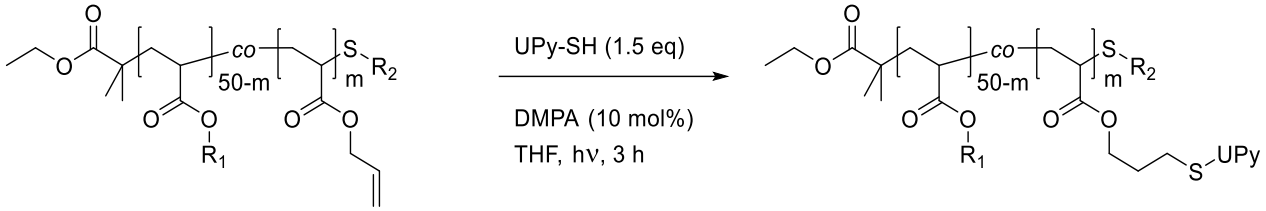

	R_1	R_2
PMA-UPy	Me	*n*-Bu
PBA-UPy	*n*-Bu	Et

Poly(methyl acrylate-co-allyl acrylate) (PMA-Allyl) or poly(butyl acrylate-co-allyl acrylate) (PBA-Allyl) (1 eq allyl esters) and UPy-SH (1.5 eq per allyl ester) were dissolved in THF (~1 M total esters). The resulting solution was degassed by argon bubbling for 30 minutes. DMPA (10 mol% per thiol) was dissolved in THF (0.2 mL) and added to the reaction mixture. After degassing for 5 more minutes, the vial with the reaction mixture was irradiated with UV light (365 nm) for 3 hours.

PMA-U5*: PMA-A5 (1.57 g, 0.92 mmol allyl-esters), UPy-SH (0.431 g, 1.38 mmol), THF (20 mL), DMPA (35.4 mg, 0.14 mmol).*
PMA-U10*: PMA-A10 (1.97 g, 2.28 mmol allyl-esters), UPy-SH (1.071 g, 3.43 mmol), THF (20 mL), DMPA (87.8 mg, 0.34 mmol).*
PMA-U15*: PMA-A15 (2.15 g, 3.61 mmol allyl-esters), UPy-SH (1.647 g, 5.27 mmol), THF (25 mL), DMPA (135.1 mg, 0.53 mmol).*

PBA-U4*: PBA-A5 (2.15 g, 0.68 mmol allyl-esters), UPy-SH (0.319 g, 1.02 mmol), THF (25 mL), DMPA (35.4 mg, 0.14 mmol).*
PBA-U9*: PBA-A9 (1.98 g, 1.39 mmol allyl-esters), UPy-SH (0.609 g, 1.95 mmol), THF (25 mL), DMPA (50.0 mg, 0.20 mmol).*
PBA-U14*: PBA-A14 (2.13 g, 2.33 mmol allyl-esters), UPy-SH (1.095 g, 3.50 mmol), THF (25 mL), DMPA (89.8 mg, 0.35 mmol).*

1.3.9 General conditions for the purification of the PMA-UPy polymers after thiol-ene coupling

The crude polymer mixture was precipitated in diethyl ether one time and, after decantation of the diethyl ether phase, the polymer was redissolved in DMF. The polymer was further purified by preparative size-exclusion chromatography with Bio-Beads S-X1 (50 g per gram of polymer) as the stationary phase and eluted with DMF. The pure fractions were combined and the solvent was removed under reduced pressure. After further drying at 80 °C under high vacuum, the polymers were compression molded at 80 °C for mechanical characterization.

1.3.10 General conditions for the purification of PBA-UPy polymers after thiol-ene coupling

The solvent of the crude polymer mixture was evaporated under vacuum and the residue was redissolved in DMF. The polymer was further purified by preparative size-exclusion chromatography with Bio-Beads S-X1 (50 g per gram of polymer) as the stationary phase and eluted with DMF. The pure fractions were combined and the solvent was removed under reduced pressure. After further drying at 80 °C under high vacuum, the polymers were compression molded at 80 °C for mechanical characterization.

2 Additional figures and tables for polymer synthesis

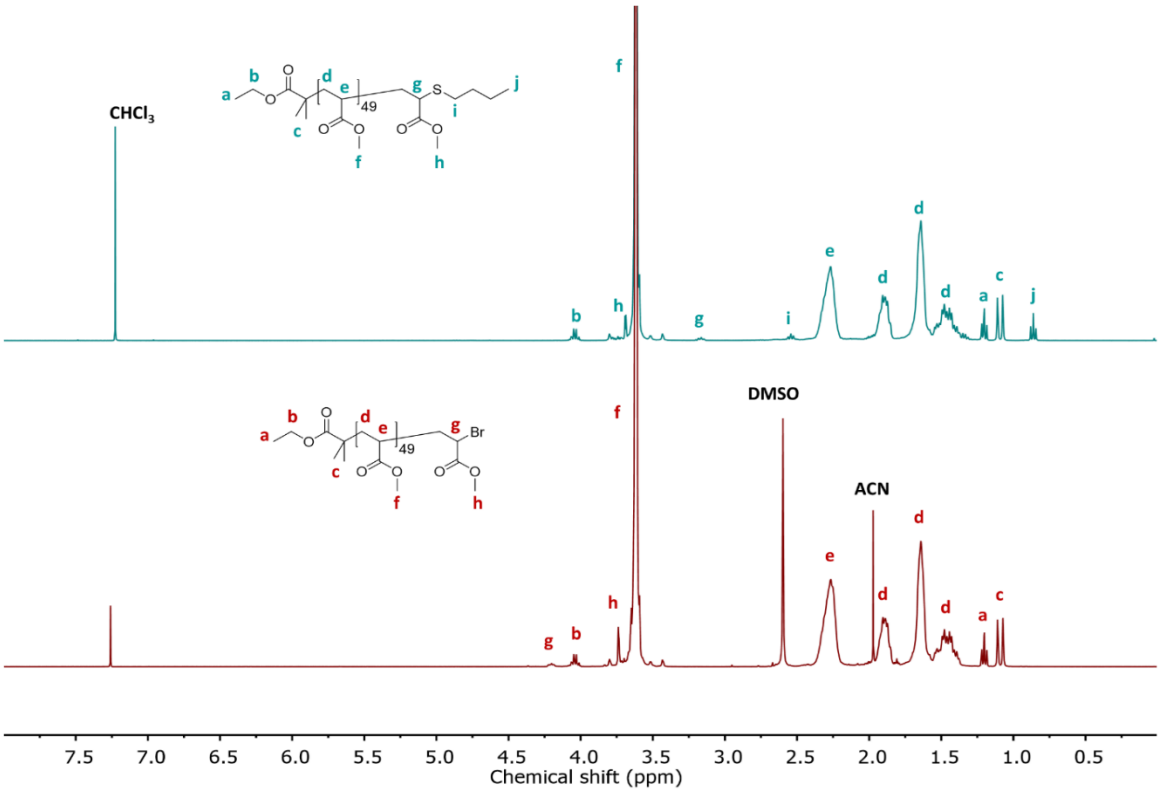

Figure S1. ^{1}H-NMR spectrum recorded in $CDCl_3$of the purified PMA isolated after polymerization (below) and after end group functionalization with 1-butanethiol (above).

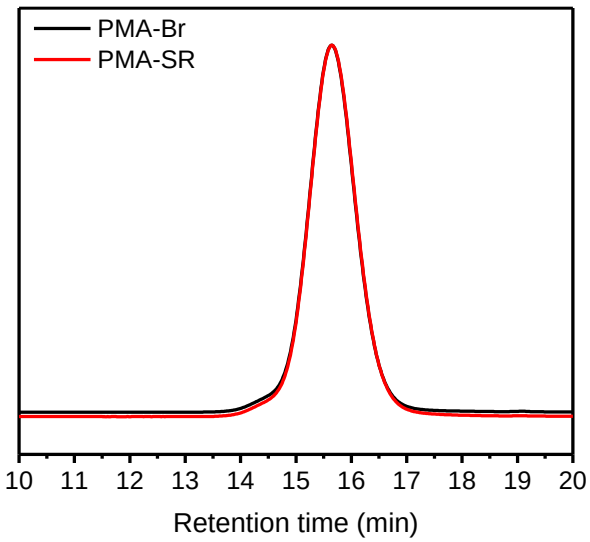

Polymer	M_n (kg/mol)	M_w (kg/mol)	Đ
PMA-Br	4.7	5.0	1.06
PMA-SR	4.8	5.1	1.06

Figure S2. Normalized SEC traces of PMA before and after end group modification with 1-butanethiol in THF (above) and the molar mass results relative to PS standards determined from the RI traces (below).

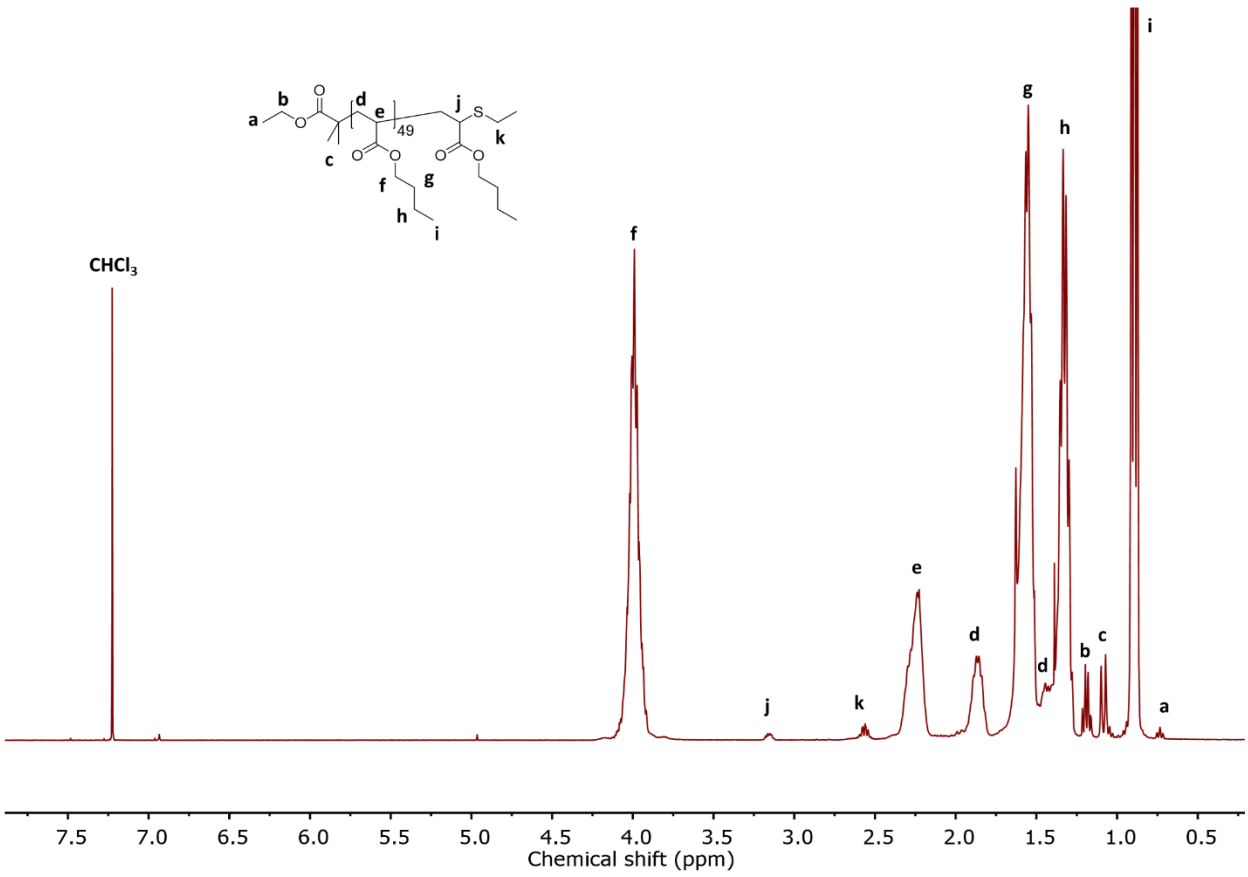

Figure S3. ^{1}H-NMR spectrum recorded in $CDCl_3$ of the purified PBA after end group functionalization with ethanethiol.

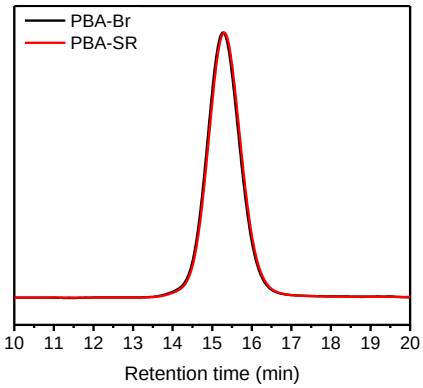

Polymer	M_n (kg/mol)	M_w (kg/mol)	Đ
PBA-Br	6.6	7.0	1.05
PBA-SR	6.8	7.1	1.05

Figure S4. Normalized SEC traces of PBA before and after end group modification with ethanethiol in THF (above) and the molar mass results relative to PS standards determined from the RI traces (below).

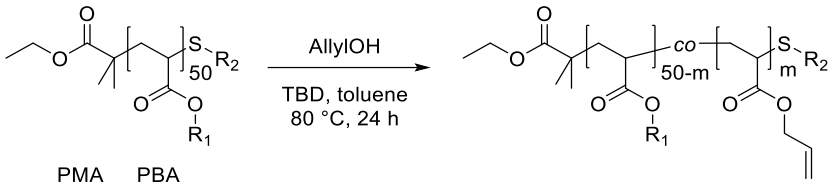

Polymer	R	Target allyl esters (%)	Stoichiometric ratio ($Eq_{AllylOH}/(1+ Eq_{AllylOH})$)	Equivalents of AllylOH	Obtained allyl esters (%)[a]
PMA-A5	Me	5	0.059	0.062	5.1
PMA-A10	Me	10	0.135	0.156	10.3
PMA-A15	Me	15	0.207	0.260	15.1
PBA-A5	*n*-Bu	5	0.059	0.062	4.8
PBA-A9	*n*-Bu	10	0.135	0.156	9.3
PBA-A14	*n*-Bu	15	0.207	0.260	13.7

Figure S5. Summary of the calculated and experimentally achieved results of the transesterification reactions on PMA and PBA as shown on top. 5 mol% of TBD per methyl or *n*-butyl ester; [a] determined using ^{1}H NMR spectroscopy.

3 Purification of the polymers

3.1 Purification of polyacrylate-allyl polymers after transesterification and thiol-ene coupling

3.1.1 Purification of the polyacrylate-allyl polymers after transesterification

After successful transesterification, the TBD catalyst had to be removed from the polymers as it could cause side reactions in the next modification step. In previous work reported by *Sumerlin* and coworkers, this was done by washing the organic phase with the polymer with an aqueous 0.1 M HCl solution.[3] However, for the allyl-functionalized PMA this resulted in a cloudy emulsion which phase separated very poorly. Consequently, a large part of the polymer was lost during work-up. To improve the polymer yield, the use of the strongly acidic exchange resin Dowex 50W X8 proved to be more efficient. The resin was added to the crude polymer solution after transesterification and the mixture was stirred at room temperature for a couple of hours. If there was still TBD left seen from the ^{1}H NMR analysis, more Dowex resin was added and the procedure was repeated until the TBD peaks completely disappeared in the ^{1}H NMR spectrum, as exemplified for PMA-A5 (**Error! Reference source not found.** main article). The PBA-Allyl polymers were purified in a n identical way as the PMA-Allyl polymers, again with complete removal of TBD as depicted in **Figure .**

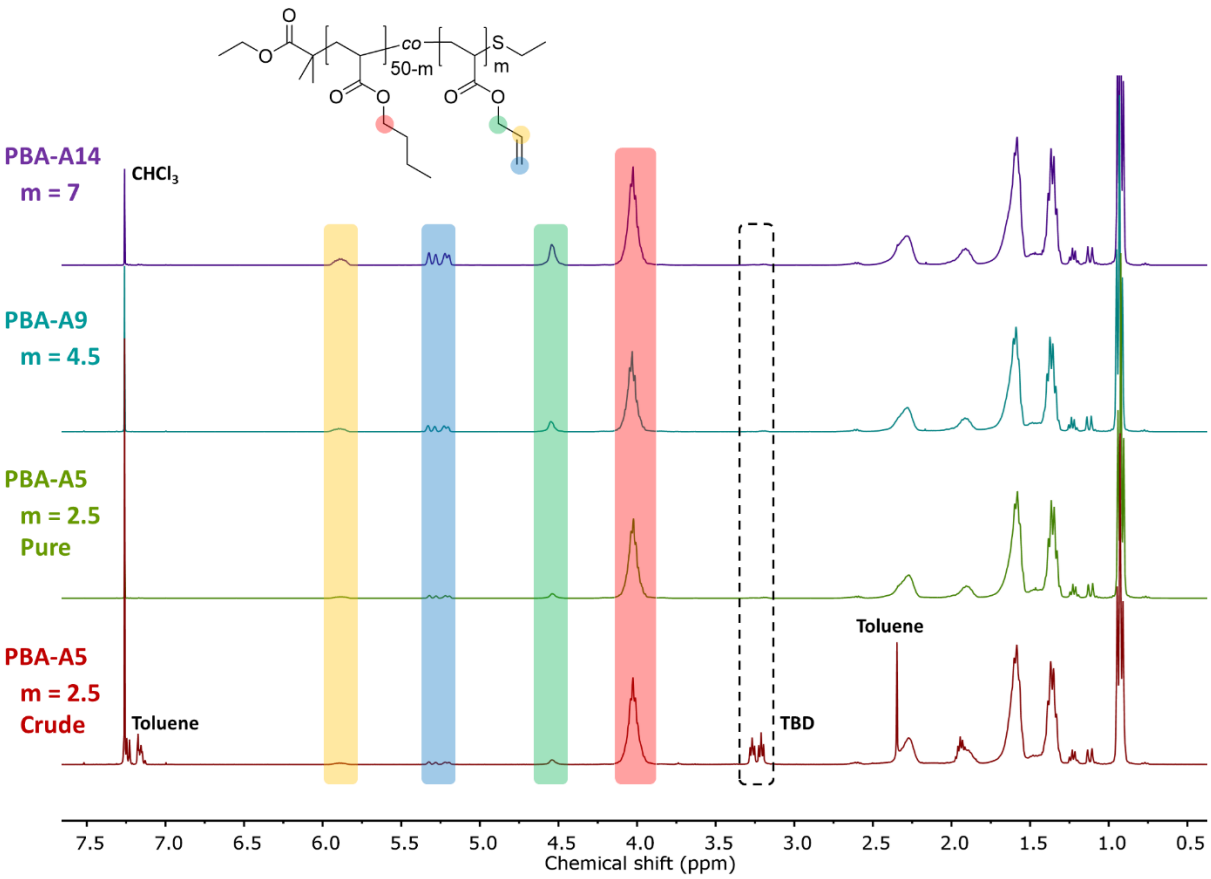

Figure S6. ^{1}H NMR spectrum recorded in $CDCl_3$of the purified PBA-Allyl polymers.

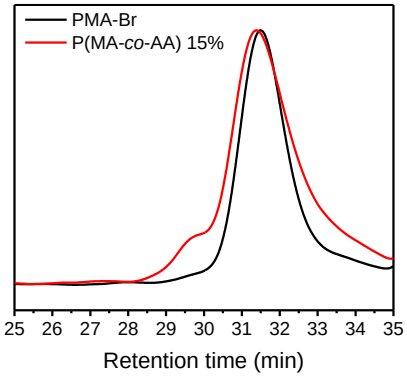

Polymer	M_n (kg/mol)	M_w (kg/mol)	Đ
PMA-Br	6.0	6.9	1.10
P(MA-co-AA) 15%	5.9	7.2	1.19

Figure S7. Normalized SEC traces of PMA with the Br end group before and after transesterification with allyl alcohol in DMA.

3.1.2 Purification of the polyacrylate-UPy polymers after thiol-ene coupling of UPy-SH

After validation of the UPy incorporation via NMR spectroscopy, the PMA-UPy polymers were analyzed further by SEC. As seen in **Figure** , the polymers retain a narrow dispersity and a clear peak shift towards higher molecular weight with increasing UPy content, consistent with the expected increase in molar mass. However, the UV signal at 300 nm clearly shows the presence of UV-active low molecular weight impurities even after precipitation in diethyl ether, suggesting incomplete removal of the excess UPy-SH. In a following purification attempt, a second precipitation in diethyl ether

was tested. However, the SEC chromatogram in **Figure** shows almost no difference with the crude sample. Next, precipitation in methanol gave better results related to the removal of excess UPy-SH, but only half of the polymer was recovered. Alternatively, a couple of functional resins with alkenes were evaluated to capture the excess of thiols. First, silica modified with acryloyl chloride was used as a cost-effective alternative for an organic resin. The crude polymer was dissolved in a 4:1 chloroform-DMF mixture and after addition of the functional silica, the suspension was reacted at room temperature overnight. After removal of the resin and precipitation in diethyl ether, SEC indicated a decrease in low molecular weight impurities, but no complete elimination of UPy-SH was observed. As a third method, a polystyrene based benzyl bromide resin was selected to exploit the thio-bromo reaction between the resin-bound benzyl bromide and UPy-SH. The polymer was dissolved in DMF and the resin was added in a 3-fold excess of 1.1 equivalents of benzyl bromide relative to the theoretical amount of thiols left after thiol-ene coupling of UPy-SH to the allyl esters. The solution with resin was stirred at room temperature for 2 days, which was also not sufficient in capturing all UPy-SH as seen in the SEC chromatogram. Potentially, disulfide formation could compromise the efficiency of the thio-bromo reaction. Therefore, the reaction with the benzyl bromide resin was repeated with an equimolar amount of dithiothreitol (DTT) relative to the remaining thiols, resulting in an improved yet incomplete removal of the UPy-SH, as observed in the SEC chromatogram in **Figure** .

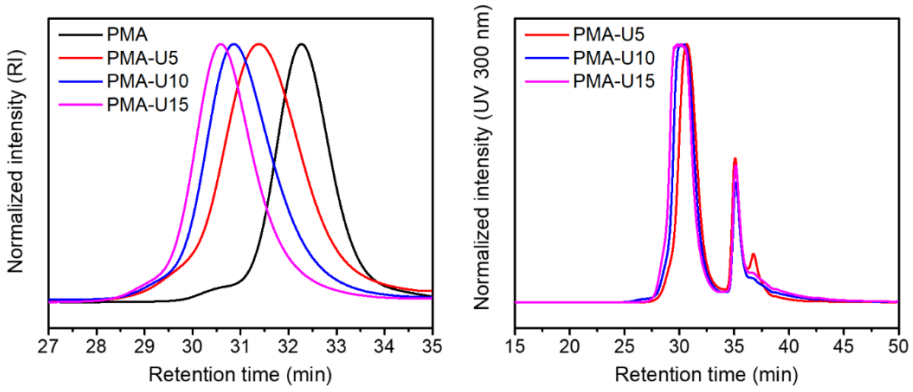

Polymer	M_n (kg/mol)	M_w (kg/mol)	Đ
PMA	8.4	8.9	1.05
PMA-U5	10.8	12.3	1.14
PMA-U10	12.9	14.4	1.12
PMA-U15	14.4	15.9	1.10

Figure S8. Normalized SEC traces of PMA before and after thiol-ene coupling of UPy-SH to PMA-Allyl measured in DMA. Upper left: Refractive index (RI) signal; upper right: UV signal at 300 nm; below: the molar mass results relative to PMMA standards determined from the RI traces.

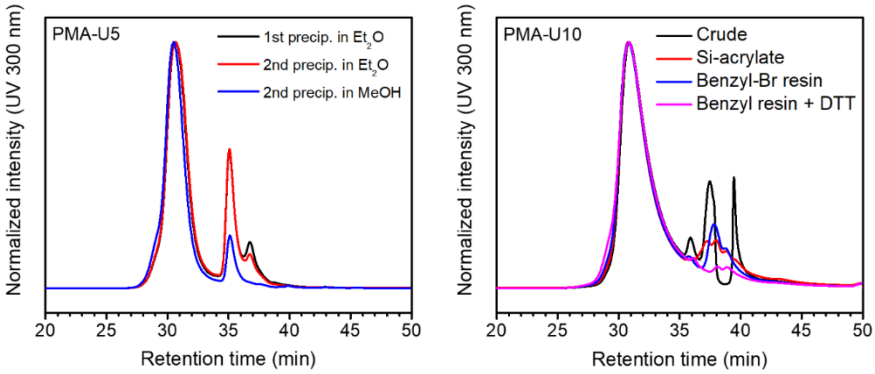

Figure S9. SEC chromatograms of the purification attempts to remove the excess UPy-SH from the PMA-UPy polymers by precipitation (left) and thiol-capturing with reactive resins (right).

In a final attempt to separate the excess UPy-SH from the polymers, preparative SEC was employed and a column was loaded with Bio-Beads S-X1 resin swollen in DMF. Dissolved in a minimal amount of DMF, the polymers were added to a column an eluted with DMF as a mobile phase and the fractions were screened for low molecular weight impurities by UV detection at 300 nm in a regular SEC analysis. As seen in **Figure** , until fraction 5 for each PMA-UPy collected, the polymer is free of UV-active impurities, which appear in increasing amount from fraction 10 onwards. For each Bio-Beads column, approximately 20% of the purified polymer could be recovered. Therefore, the impure fractions which contained a significant amount of polymer were combined and purified two more times to obtain enough material for mechanical characterization of the hydrogen bonded polymer networks.

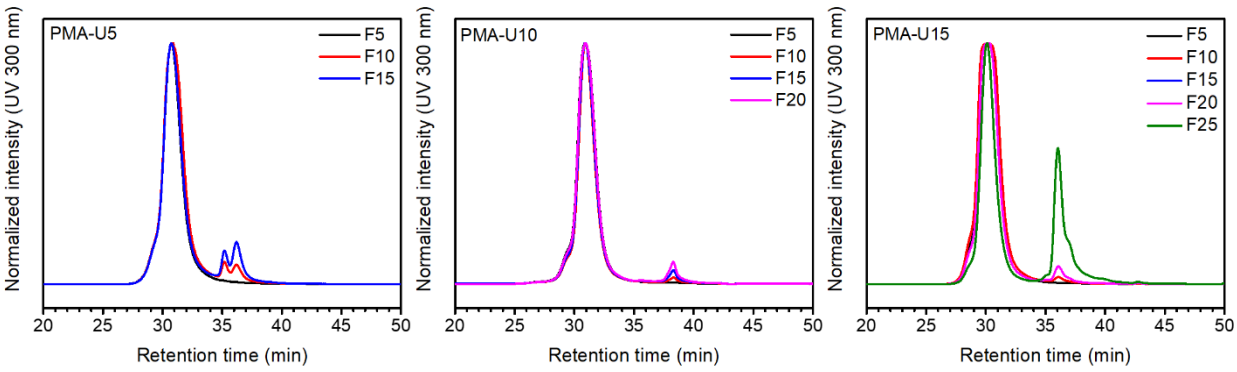

Figure S10. SEC chromatograms of different fractions (F) eluted during preparative SEC over Bio-Beads S-X1 in DMF performed on the PMA-UPy polymers.

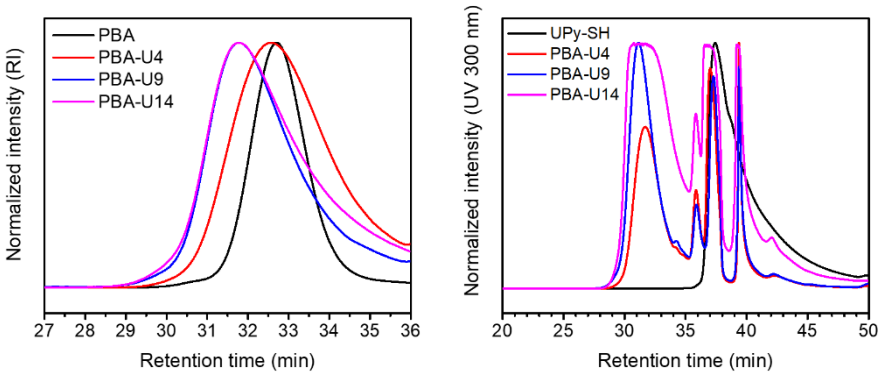

Polymer	M_n (kg/mol)	M_w (kg/mol)	Đ
PBA	3.8	4.4	1.15
PBA-U4	3.4	4.4	1.31
PBA-U9	4.2	5.6	1.34
PBA-U14	3.4	5.3	1.56

Figure S11. Normalized SEC traces of PBA before and after thiol-ene coupling of UPy-SH to PBA-Allyl measured in DMA. Upper left: Refractive index (RI) signal; upper right: UV signal at 300 nm; below: the molecular weight results relative to PMMA standards determined from the RI traces.

The PBA-UPy polymers were purified by preparative SEC as described above for the PMA-UPy polymers. Each polymer was run over the column three times to isolate enough material for the characterization of the mechanical properties, the pure fractions were combined and most DMF was evaporated under reduced pressure. **Figure** displays the SEC analysis of different fractions taken during separation over Bio-Beads and illustrates the successful purification of the polymers up to fraction 5, and the impurities starting to elute from fraction 10 onwards. After drying under high vacuum at 80 °C for 24 hours, the polymer networks were analyzed by ^{1}H NMR spectroscopy to ensure complete removal of DMF. Indeed, the ^{1}H NMR spectra are free of solvent impurities and the materials are suitable for mechanical characterization.

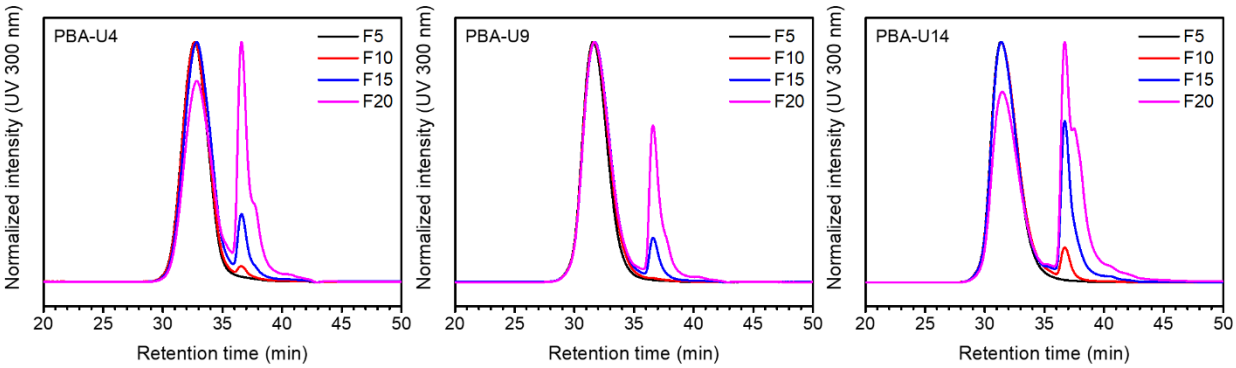

Figure S12. SEC chromatograms of different fractions eluted during preparative SEC over Bio-Beads S-X1 in DMF performed on the PBA-UPy polymers.

4 Rheology of Supramolecular Polymers

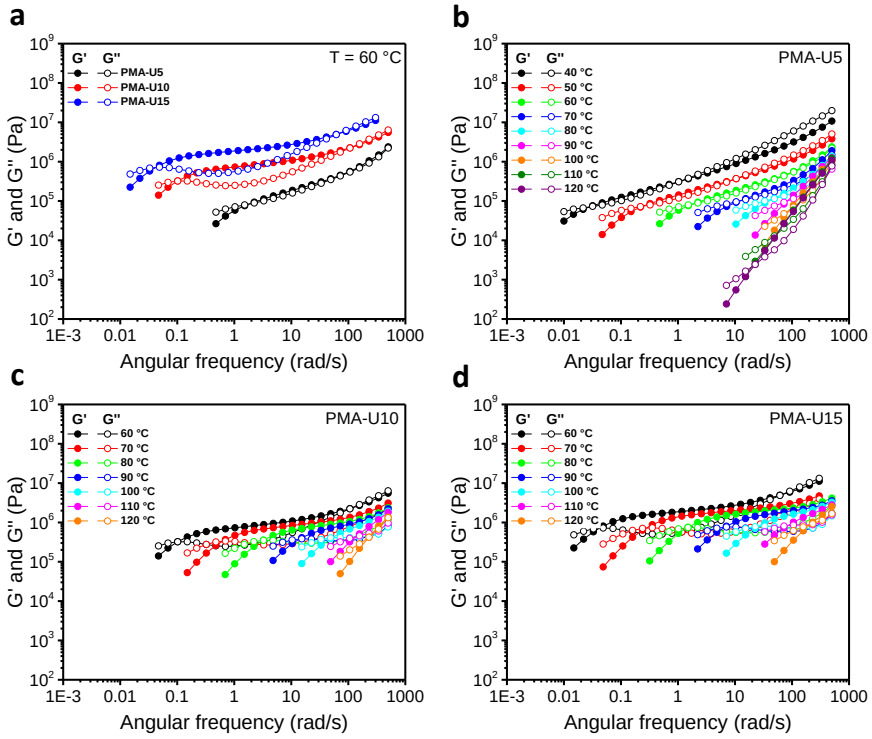

Figure S13. Frequency sweeps showing G' and G'' as a function of the angular frequency for the PMA-UPy materials. a) PMA-U5, PMA-U10, and PMA-U15 at 60 °C; b) PMA-U5 at 40-120 °C; c) PMA-U10 at 60-120 °C; d) PMA-U15 at 60-120 °C.

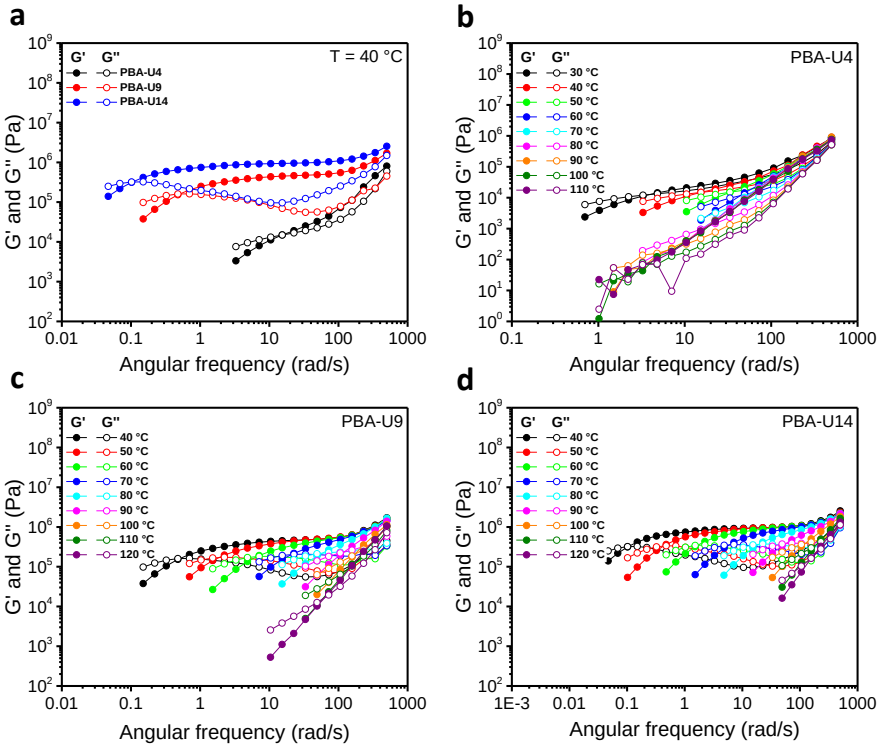

Figure S24. Frequency sweeps showing G' and G'' as a function of the angular frequency for the PBA-UPy materials. a) PBA-U4, PBA-U9 an PBA-U14 at 40 °C; b) PBA-U4 at 30-120 °C; c) PBA-U9 at 40-120 °C; d) PBA-U14 at 40-120 °C.

5 Modelling the Linear Rheology of Supramolecular Polymers

In unentangled polymers with pendants associative groups, the relaxation behavior is highly influenced by the average number of associating groups per chain $\boldsymbol{N_s}$.[4–6] When $\boldsymbol{N_s}$ exceeds 2, the chains become interconnected, resulting in the formation of a network. The "sticky Rouse" model was introduced to explain the linear viscoelasticity in this regime.[6] In this model, which has been extensively used in the literature to fit the linear viscoelastic response of unentangled supramolecular polymers,[7–9] the spectrum of relaxation times is divided into two groups. First, the "fast modes" accounts for the relaxation of subchains smaller than the mean length between two associative bonds, of molar mass $\boldsymbol{M_s}$. These fast modes follow the Rouse relaxation of the precursors. Then, the "slow modes" involve the relaxation of subchains that are larger than $\boldsymbol{M_s}$. These relaxation modes are uniformly delayed by the side-groups and thus are described by a slower Rouse process referred to as "Sticky Rouse". It has been found that the model provides a decent fit of the experimental results of the here reported UPy functionalized polyacrylates. However, substantial discrepancies were observed in the rubbery plateau region and in the terminal regime.[8] Different causes for these discrepancies have been proposed and investigated in the literature. First, the sticky Rouse model assumes a uniform distribution of the supramolecular junctions along the chains. This is in contrast with the random placement of the junctions that is frequently obtained with the synthesis processes of the associative systems. The models of Cui et al.[8] and Liu et al.[10] include these inhomogeneities, which allowed to obtain a better description of the data in the terminal regime. However, even with these improvements, it is not sufficient to describe accurately the relaxation of unentangled associative polymers.

Indeed, Liu et *al.*[10] provided an explanation for the persistent deviations by stating that the bounded stickers have the ability to diffuse over a certain distance, thereby partially relieving the stress. Subsequently, they integrated these non-affine spatial fluctuations into the sticky Rouse model using a phenomenological approach. This integration allowed to obtain an accurate fit of the linear data of unentangled melt data for two distinct copolymer chemistries at varying concentrations of supramolecular associations. Notably, their model maintains the crucial assumption that the fluctuations do not affect the level of the rubbery plateau. This important hypothesis is in agreement with the earlier work of Indei and Takimoto[11] who analytically treated the effect of the junction fluctuations on the rubbery plateau.

Finally, part of the divergences could also emanate from the presence of a distribution of sticker lifetimes, as postulated by Cui et *al.*[8] The introduction of such distribution can be justified by adopting arguments similar to the ones used in the bond lifetime renormalization model.[6] This model predicts different lifetime $\boldsymbol{\tau_S}$ for associative polymers containing different densities of stickers. One could therefore expect that the fluctuations in density of stickers along the polymeric chains also lead to a multitude of lifetimes. Moreover, as explained by Cui *et al.*[8], when the supramolecular junctions are in close proximity, the segments between two associative groups may lack the required flexibility for the associative groups to effectively search for potential partners within their exploration volume. Consequently, in order to exchange partners, it may be necessary for multiple junctions to dissociate simultaneously, leading to an increase in the exploration volume and thus in the number of potential partners.

Unentangled chains relax through the Rouse process. In this model, the polymeric chains are viewed as a series of N beads of friction ζ_0 attached to each other via $N-1$ massless springs. Each spring contains g Kuhn segments with $g \geq 1$.[12] Similarly to Jiang *et al.*[13], the Rouse model is extended to unentangled associative polymers through the effective friction concept. This means that the supramolecular junctions are assimilated to beads of high friction, as shown in Error! Reference source not found.**5**.

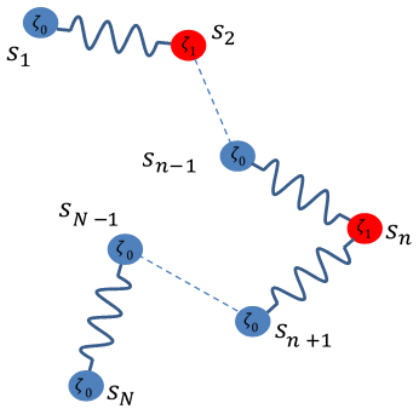

Figure S15. Illustration of the bead-spring model, featuring blue beads with a friction coefficient ζ_0 and red beads with a higher friction coefficient ζ_1.

The position of the nth bead $\boldsymbol{r}(n,t)$ at time t is therefore described by the following Langevin equation. [12,14]

$$\zeta(n)\frac{\partial \boldsymbol{r}(n,t)}{\partial t} = -\kappa \sum_{m=0}^{N} A_{nm}\boldsymbol{r}(n,t) + \boldsymbol{F_B}(n,t) \tag{1}$$

Here $\zeta(\mathrm{n})$ is the friction coefficient of the n^{th} bead, κ is the spring constant, A_{nm} is the Rouse matrix and $\mathbf{F_B}$ is the Brownian force. The Rouse matrix A_{nm} accounts for the connectivity of the chains and is given by the Laplacian matrix.[15]

Thus, for a linear chain, A_{nm} can be written as

$$\mathbf{A} = \begin{bmatrix} 1 & -1 & & & \\ -1 & 2 & -1 & & \\ & & \ldots & & \\ & & -1 & 2 & -1 \\ & & & -1 & 1 \end{bmatrix} \tag{2}$$

The first and second moments of $\mathbf{F_B}$ are given by

$$\begin{gathered} \langle \mathbf{F_B}(n,t) \rangle = 0 \\ \langle \mathbf{F_B}(n,t)\mathbf{F_B}(m,t') \rangle = 2\zeta_{\mathrm{eq}}(n)\mathrm{k_B T}\delta_{\mathrm{nm}}\delta(\mathrm{t}-\mathrm{t}')\mathbf{I} \end{gathered} \tag{3}$$

In the last equality, the Brownian force intensity is given by the fluctuation-dissipation theorem.

5.1 Decoupling of the Normal Modes

In the present work, the model of Liu *et al.*[10] is employed. In their model, the solution of equation (2) is approximated by decoupling the long-term dynamics from the short-term dynamics. This hypothesis is valid provided that $N_s^2\tau_S \gg N^2\tau_0$. This inequality indicates that the friction of the backbone must be significantly lower than the friction introduced by the stickers.

A. Fast Relaxation Modes

At short times, the network strands relax through the non-sticky Rouse process. The dynamic moduli are given by

$$G'(\omega) = \beta\frac{\rho RT}{M}\sum_{p=1}^{N-1}\frac{\left(\omega\tau_{R,p}\right)^2}{1+\left(\omega\tau_p\right)^2} \tag{4}$$

$$G''(\omega) = \beta\frac{\rho RT}{M}\sum_{p=1}^{N-1}\frac{\omega\tau_{R,p}}{1+\left(\omega\tau_{R,p}\right)^2} \tag{5}$$

Here, the relaxation time $\tau_{R,p}$ is expressed as

$$\tau_{R,p} = \frac{1}{4\sin^2\left(\frac{p\pi}{2N}\right)}\frac{\zeta_0}{\kappa_0} \qquad p = 1,\ldots,N-1 \tag{6}$$

where $\frac{\zeta_0}{\kappa_0}$ represents a characteristic time related to the segmental motion of the chains.

Equations (4) and (5) introduce a deviation from the classical sticky Rouse theory by starting the sum over the Rouse modes at $p = 1$ instead of $p = S$. According to Liu et al.[10], this adjustment enables correction for the spatial fluctuations of the stickers. Consequently, the sum now includes $N-1$ modes rather than the $N-1-S$ modes as obtained in the classical theory. To ensure consistency between the number of modes and the number of beads, we introduced a normalization constant $\beta = \frac{N-1-S}{N-1}$ in equation (4) and (5).

B. Slow Relaxation Modes

At long times, the flow dynamics is primarily governed by the motion of the sticky beads. The bead-spring chain depicted in Error! Reference source not found.**5** can therefore be replaced with a chain consisting solely of sticky beads. As a r esult, the long-time chain dynamics is described by the following set of equations.

$$\zeta_1 \frac{d\boldsymbol{q_1}}{dt} = \kappa_1(R_2 - R_1) + f_1 \tag{7}$$

$$\zeta_1 \frac{d\boldsymbol{q_i}}{dt} = \left(\kappa_i(R_{i+1} - R_i) - \kappa_{i-1}(R_i - R_{i-1})\right) + f_i \tag{8}$$

$$\zeta_1 \frac{d\boldsymbol{q_S}}{dt} = \kappa_{S-1}(R_{S-1} - R_S) + f_i \tag{9}$$

Here, $\boldsymbol{q}_i$ denotes the position of the i^{th} sticky beads and κ_i represents the corresponding elastic constants.
When the stickers are equally spaced along the chains, the elastic constant of the strands are given by

$$\kappa = \frac{3k_BT}{Nb^2}(S-1), \tag{10}$$

where k_B is the Boltzman constant and T the absolute temperature.
In contrast, when the supramolecular junctions are distributed randomly, the elastic constant of the springs connecting the $i-1^{th}$ and i^{th} sticky beads is given $\kappa_i = \alpha_i\kappa$ with α_i equal to

$$\alpha_i = \frac{N}{n_i(N_s - 1)}, \tag{11}$$

where n_i represents the number of Rouse segments on the i^{th} strand of the polymeric chain.
The solution to this set of equations yields the following expressions for the dynamic moduli.

$$G'(\omega) = \frac{\rho RT}{M}\sum_{p=1}^{S-1}\frac{\left(\omega\tau_p\right)^2}{1+\left(\omega\tau_p\right)^2} \tag{12}$$

$$G''(\omega) = \frac{\rho RT}{M}\sum_{p=1}^{S-1}\frac{\omega\tau_p}{1+\left(\omega\tau_p\right)^2} \tag{13}$$

Here, the relaxation time τ_p is determined by the ratio $\frac{\zeta_1}{\kappa_1\lambda_p}$ with $\frac{\zeta_1}{\kappa_1}$ being a characteristic time associated the supramolecular bonds and the λ_p being the p^{th} highest nonzero eigenvalues of the matrix $\boldsymbol{\Lambda}$.

$$\boldsymbol{\Lambda} = \begin{bmatrix} \alpha_1 & -\alpha_1 & 0 & \dots & \dots & 0 \\ -\alpha_1 & \alpha_1 + \alpha_2 & -\alpha_2 & 0 & \dots & 0 \\ \dots & \dots & \dots & \dots & \dots & \dots \\ 0 & \dots & 0 & -\alpha_{S-2} & \alpha_{S-2} + \alpha_{S-1} & -\alpha_{S-1} \\ 0 & \dots & \dots & 0 & -\alpha_{S-1} & \alpha_{S-1} \end{bmatrix} \tag{14}$$

5.2 Distribution of Sticky Beads and Molecular Weight

To account for the random placement of the stickers, an ensemble of R chains of N beads was generated. Each bead in the chains has a probability P of being associative. The length of each network strands m is computed based on the following geometric distribution.

$$p(X = m) = P(1-P)^{m-1} \tag{15}$$

To obtain the lengths of the network strands in a specific chain, we repeatedly compute values of length using the probability distribution defined by equation (15) until the cumulative sum surpasses the total number of beads N. The resulting series of strand lengths determines the placement of the stickers, starting from one end of the chain.

Error! Reference source not found. presents the distribution of the number of sticky beads per chain and the d istribution of strand length obtained using $R = 30000$ and $N = 100$ for various values of λ, the average number of associated stickers per chain. In panel (a), it can be observed that when N is significantly large, the distribution of the number of sticky beads closely approximates the following Poisson distribution:

$$p(X = m) = \frac{\lambda^m \exp(-\lambda)}{m!} \qquad \text{with } \lambda = PN \tag{16}$$

As observed in **panel b)**, there is significant probability of having sticky beads close to each other. As suggested by Cui et al.[16], this proximity could lead to the presence of stronger physical bonds as multiple pairs of stickers would need to detach simultaneously to relax the stress. It is worth mentioning that this effect is not considered in the present work.

Finally, a log-normal distribution is used to characterize the distribution of molecular weights, following a similar approach as reported previously.[17]

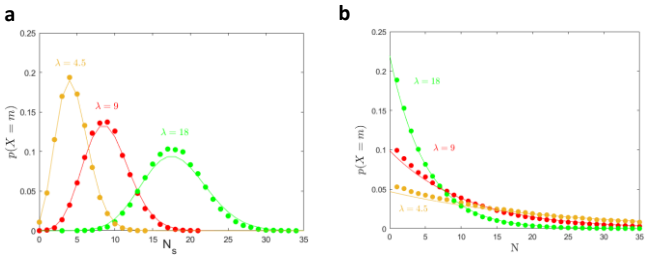

Figure S16. a) Distribution of the number of sticky beads per chain for three different values of λ. b) Distribution of the length of the network strands per chain for three different values of λ. The solid lines show the corresponding a) Poisson distributions and b) geometric distributions. The full circles were obtained using $R = 30000$ and $N = 100$.

5.3 Glassy relaxation

In order to model the glassy part, the phenomenological Kohlrausch–Williams–Watts (KWW) model is used. Its expression in the frequency domain is given by[18]

$$G'_{KWW}(\omega) = \omega G_g \int_0^\infty \exp\left(-\left[\frac{t}{\tau_{KWW}}\right]^\beta\right) \sin(\omega t)\, dt \tag{17}$$

$$G''_{KWW}(\omega) = \omega G_g \int_0^\infty \exp\left(-\left[\frac{t}{\tau_{KWW}}\right]^\beta\right) \cos(\omega t)\, dt \tag{18}$$

Here, three fitting parameters are introduced: the glassy modulus G_g, the characteristic time of the glassy relaxation τ_{KWW} and the stretch parameter β. The latter specifies the broadness of the distribution of the glassy modes. A decreasing β leads to a broader distribution.

5.4 Prediction of rheological behavior

Figure S7 shows the prediction of the model detailed above. The fitting parameters are listed in **Table 5**, main manuscript. Following *Fetters et al.*,[19] a M_k of 120 g/mol have been used to model the responses of the PB polymers. A density of $\rho = 1000$ kg/m^3 was also assumed.

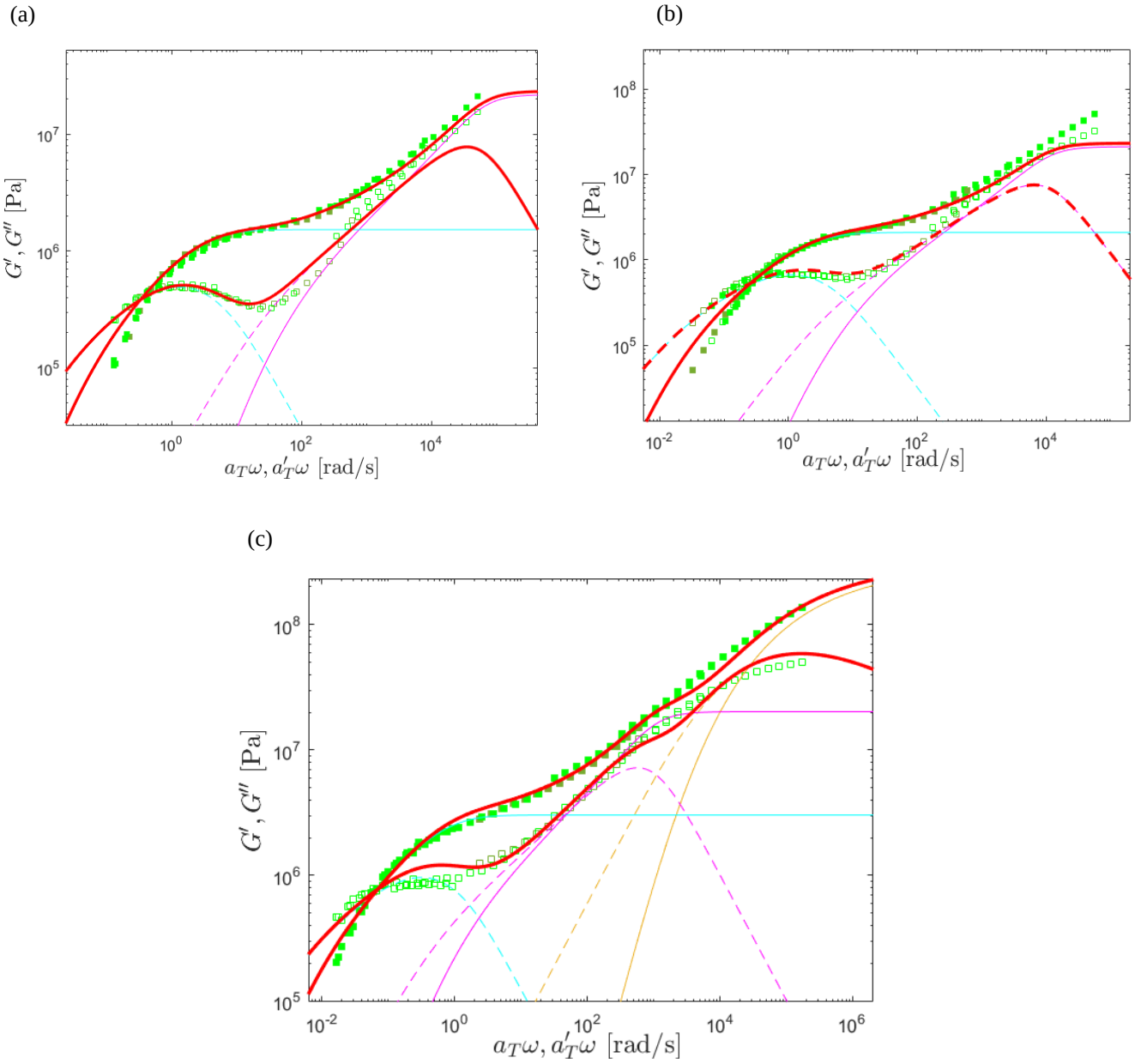

Figure S17. Linear viscoelastic mastercurves of PB-U6 (a), PB-U8 (b) and PB-U13 (c) at $T_{ref} = 80$°C. Red lines correspond to the model predictions with and without fluctuations obtained with the parameters shown in Table 1 and 2. The contributions from the KWW model (in orange), the Rouse model (in magenta) and the slow modes (in cyan) are also presented.

6 References

1 H. M. Keizer, R. P. Sijbesma and E. W. Meijer, *Eur. J. Org. Chem.*, 2004, **2004**, 2553–2555.
2 J. F. R. Van Guyse, Y. Bernhard and R. Hoogenboom, *Macromol. Rapid Commun.*, 2020, **41**, 2000365.
3 C. P. Easterling, T. Kubo, Z. M. Orr, G. E. Fanucci and B. S. Sumerlin, *Chem. Sci.*, 2017, **8**, 7705–7709.
4 Z. Zhang, Q. Chen and R. H. Colby, *Soft Matter*, 2018, **14**, 2961–2977.
5 Q. Chen, C. Huang, R. A. Weiss and R. H. Colby, *Macromolecules*, 2015, **48**, 1221–1230.
6 M. Rubinstein and A. N. Semenov, *Macromolecules*, 1998, **31**, 1386–1397.
7 Q. Chen, G. J. Tudryn and R. H. Colby, *J. Rheol.*, 2013, **57**, 1441–1462.
8 G. Cui, V. A. H. Boudara, Q. Huang, G. P. Baeza, A. J. Wilson, O. Hassager, D. J. Read and J. Mattsson, *J. Rheol.*, 2018, **62**, 1155–1174.
9 A. Shabbir, I. Javakhishvili, S. Cerveny, S. Hvilsted, A. L. Skov, O. Hassager and N. J. Alvarez, *Macromolecules*, 2016, **49**, 3899–3910.
10 H. Liu, G. Ianniruberto and G. Marrucci, *J. Rheol.*, 2022, **66**, 1183–1190.
11 T. Indei and J. Takimoto, *J. Chem. Phys.*, **133**, 19402.
12 A. E. Likhtman, in *Polymer Science: A Comprehensive Reference*, Elsevier, 2012, pp. 133–179.
13 N. Jiang, H. Zhang, P. Tang and Y. Yang, *Macromolecules*, 2020, **53**, 3438–3451.
14 R. G. Larson, *Constitutive Equations for Polymer Melts and Solutions*, Butterworth-Heinemann, London, 1988.
15 Y. Yang, *Macromol. Theory Simulations*, 1998, **7**, 521–549.
16 G. Cui, V. A. H. Boudara, Q. Huang, G. P. Baeza, A. J. Wilson, O. Hassager, D. J. Read and J. Mattsson, *J. Rheol.*, 2018, **62**, 1155–1174.
17 J. Verjans, A. André, E. Van Ruymbeke and R. Hoogenboom, *Macromolecules*, 2022, **55**, 928–941.
18 G. Williams and D. C. Watts, *Trans. Faraday Soc.*, 1970, **66**, 80.
19 L. Fetters, *Physical Properties of Polymers Handbook*, Springer: New York, 2007.